

Single ion scattering contributions to the thermal conductivity of LiHoF_4 and $\text{LiY}_{96\%}\text{Ho}_{4\%}\text{F}_4$

James Nikkel and Brett Elman^y
 Kent State University, 105 Smith Laboratory, Kent, OH
 (Dated: March 23, 2024)

We have performed extensive zero-field thermal conductivity measurements on single crystal samples of LiHoF_4 and $\text{LiY}_{96\%}\text{Ho}_{4\%}\text{F}_4$ below 2.3 K. By comparing these data to a single ion scattering model, we have shown that the thermal conductivity of $\text{LiY}_{96\%}\text{Ho}_{4\%}\text{F}_4$ is dominated by simple single-ion scattering while that of LiHoF_4 shows additional contributions, possibly associated with collective spin excitations. No entirely satisfactory model, however, is available to explain the thermal conductivity of the ferromagnet.

I. INTRODUCTION

LiHoF_4 has been the focus of numerous experimental and theoretical studies^{1,2}. The crystal field constrains the angular momentum of the Ho^{3+} ions to lie strictly along the c-axis. Furthermore, the large Ho-Ho spacing greatly reduces the exchange term, making the system an excellent approximation to a model dipolar Ising ferromagnet. The non-magnetic ion Y^{3+} substitutes isostructurally and isoelectronically for Ho^{3+} , leading to dilute 3-d Ising systems. The latter are, for low magnetic ion concentrations, known to form a puzzling glassy system at low temperatures, whose signature is a narrowing distribution of barriers to relaxation as temperature is lowered. One goal of measuring thermal conductivity in these systems is to obtain coarse phonon spectroscopic data to probe the Ho^{3+} ion energy levels in the low-temperature glass and ferromagnet. Indeed, the LiHoF_4 and $\text{LiY}_{96\%}\text{Ho}_{4\%}\text{F}_4$ characteristic hyperfine and magnetic energy level spectra are measured in the 100's of milli-Kelvins, making thermal phonons at temperatures $\sim 1\text{K}$ an experimentally simple way to access the characteristic energies of the system (simple, that is, when compared to, e.g., millimeter photon spectroscopy). The central questions we ask are (a) whether low-temperature collective excitations exist in the Ising ferromagnet LiHoF_4 below $T_c = 1.53\text{K}$ and (b) whether the anomalous glassy behavior of the dilute system $\text{LiY}_{96\%}\text{Ho}_{4\%}\text{F}_4$ is due to rearrangements of correlated spin clusters. In order to address these issues, we must analyze the data in such a way as to deconvolve the rather complex single Ho^{3+} ion contribution to the thermal resistance. We will accomplish this via a detailed analysis of the crystal field splittings and resulting single-ion excitations that cause phonon scattering.

II. SCATTERING MODEL

We start with the general form of the thermal conductivity, κ , in terms of the phonon heat capacity, $C(k)$, the mean free path, $l(k)$, and the speed of sound, $v(k)$, written as an integral over the phonon wave vector, k :

$$\kappa = \int \frac{d^3k}{(2\pi)^3} C(k) v(k) l(k) \quad (1)$$

Our initial approximations are to assume that the system is structurally isotropic with respect to k and that only acoustic phonons with a linear dispersion relation contribute at the experimental temperatures. We can then calculate the thermal conductivity in terms of an integral over the phonon frequency, ω , as

$$\kappa = \frac{4}{v^2} \int \omega^2 C(\omega) l(\omega) d\omega \quad (2)$$

The specific heat, $C(\omega)$ contribution from phonons with energy between ω and $\omega + d\omega$, is the derivative of the mean thermal energy density of the lattice³,

$$C(\omega) d\omega = \frac{d}{dT} \left(\frac{1}{8\pi^3} \int \frac{h\omega}{e^{h\omega/k_B T} - 1} d^3k \right) \quad (3)$$

Using equation 2, the thermal conductivity is now

$$\kappa = \frac{h^2}{2\pi^2 v^2 k_B T^2} \int_0^\infty \omega^4 \frac{e^{h\omega} l(\omega) d\omega}{(e^{h\omega} - 1)^2} \quad (4)$$

Our task is to find $l(\omega)$, taking into account both single-ion magnetic scattering and scattering due to, e.g., crystalline defects. For reference, we reproduce in table II a synopsis³ of the ω dependence of various structural scattering mechanisms.

We also assume the correctness of Matthiessen's rule, i.e., that contributions to the mean free path are added reciprocally.

III. DETAILED SINGLE ION CALCULATION

The thermal resistance of an isolated Ho^{3+} ion may be numerically estimated from the electronic transition probabilities of the ions when they are excited by thermal phonons. We will not attempt here to calculate from first

Type of scattering	$l(!) /$	$(T) /$
External boundaries	const:	T^3
Grain boundaries	const:	T^3
Stacking faults	$!^2$	T
Conduction electrons	$!$	T^2
Point defects	$!^4$	$l=T$
Umklapp processes	$!$	$T^3 e^{-T}$

TABLE I: Table of the functional form of the mean free path, l , on $!$.

principles the electron-phonon coupling constants. Instead, we will use a semi-phenomenological model to ascertain whether a single-ion scattering term can account for the observed thermal conductivity. The 5I_8 multiplet of the Ho^{3+} ions in $LiHoF_4$ is comprised of a ground state doublet followed by two singlets at about 9 and 39 K. The energy levels above these are of sufficiently high energy that we can neglect them at the experimental temperatures. The ground state doublets are each split into 8 hyperfine sublevels which in turn may be split relative to each other due to a Zeeman interaction with an external or internal magnetic field. The magnitude of the ground state magnetic splitting in the ferromagnet was measured by Battison et al.⁴. Using an optical spectroscopic technique, they found it to be proportional to the magnetization (i.e., mean field) with a maximum at zero temperature equal to 2.6 cm^{-1} , or 3.7 K.

The energy levels are calculated by solving the eigenvalue problem for the 5I_8 single ion Hamiltonian. We follow the method described by Giraud et al.⁵. In the $|j; m; I; n\rangle$ basis, the Hamiltonian can be approximated as the sum of the crystal field, Zeeman, and hyperfine contributions,

$$H = H_{CF} + H_{Ze} + H_{hf} : \quad (5)$$

The crystal field contribution is written in terms of the Stevens' operators, O_1^m , and the crystal field parameters, B_1^m . The resulting crystal field Hamiltonian is

$$H_{CF} = B_2^0 O_2^0 + B_4^0 O_4^0 + B_4^4 O_4^4 + B_6^0 O_6^0 + B_6^4 O_6^4 ; \quad (6)$$

where B_2^0 , B_4^0 , and B_6^0 are ion specific coefficients calculated by Stevens⁶. For Ho^{3+} , $B_2^0 = 1450$, $B_4^0 = 130030$, and $B_6^0 = 13864861$. (The general form for B_4^4 and B_6^4 can be found on page 253 of Hutchings⁷.) The crystal field parameters, B_1^m , are given by Giffelman et al. in reference⁸ and were measured through high resolution optical spectroscopy. Their values are: $B_2^0 = 273.9 \text{ K}$, $B_4^0 = 97.7 \text{ K}$, $B_6^0 = 6.5 \text{ K}$, $B_4^4 = 1289.1 \text{ K}$, and $B_6^4 = 631.6 \text{ K}$.

O_1^m	in $ j; m; I; n\rangle$ basis
O_2^0	$3J_z^2 - J(J+1)$
O_4^0	$35J_z^4 - 30J(J+1)J_z^2 + 25J_z^2$ $6J(J+1) + 3J^2(J+1)^2$
O_4^4	$\frac{1}{2} J_+^4 + J_-^4$
O_6^0	$231J_z^6 - 315J(J+1)J_z^4$ $+ 735J_z^4 + 105J^2(J+1)^2J_z^2$ $525J(J+1)J_z^2 + 294J_z^2$ $5J^3(J+1)^3 + 40J^2(J+1)^2$ $60J(J+1)$
O_6^4	$\frac{1}{4} 11J_z^2 - J(J+1) - 38 J_+^4 + J_-^4$ $+ J_+^4 + J_-^4 - 11J_z^2 - J(J+1) - 38$

TABLE II: Table of the Stevens' operators and equivalents.

The Stevens' operators, O_1^m are given in reference 6 and 7 and the ones of interest here are summarized in table III.

The Zeeman contribution to the Hamiltonian is simply

$$H_{Ze} = g_J \mu_B \mathbf{J} \cdot \mathbf{H} \quad (7)$$

where the g-factor $g_J = 5/4$ for the $J = 8$ ground state, μ_B is the Bohr magneton, and \mathbf{H} is the magnetic field due to applied external fields and the internal field in the ferromagnetic state. Due to the symmetry of the crystal, the internal magnetic field due to ferromagnetic order is directed along the (Ising) c axis. Therefore, in the absence of an external field, and within the mean-field approximation, we may write

$$H_{Ze} = g_J \mu_B \frac{H_0}{M_0} M(T) J_z ; \quad (8)$$

where M_0 is the saturation magnetization at zero temperature, H_0 is the effective maximum internal field at zero temperature, and $M(T)$ is the temperature dependent magnetization. Note that this is the only term in the Hamiltonian where the temperature enters into the calculation of the energy spectrum. (The thermal broadening of energy levels described below also depends on T .) The magnetization of $LiHoF_4$ is calculated from α to the magnetization data measure in reference 9. The zero temperature internal field, H_0 , is approximately 0.33 T which gives the correct splitting of 3.7 K at zero temperature as measured by Battison et al. 4. Note that since our sample geometry is a long bar along the c-axis, we do not apply a demagnetization correction.

The hyperfine contribution may be written

$$H_{hf} = A_J \mathbf{J} \cdot \mathbf{I} : \quad (9)$$

The coupling parameter A_J was found to be approximately 39 mK by Mennenga et al.¹⁰ for $LiHoF_4$ from specific heat measurements. Magarino et al.¹¹ found approximately the same value for 2% Ho^{3+} diluted into $LiYF_4$ using electron paramagnetic resonance.

For the Ho^{3+} ions in LiHoF_4 and $\text{LiY}_{96\%}\text{Ho}_{4\%}\text{F}_4$, $J = 8$ and $I = 7/2$. Therefore, the Hamiltonian takes the form of a 136×136 Hermitian matrix. Numerical diagonalization gives the respective eigenvectors, which in turn allow the calculation of pertinent expectation values. Specifically, it is important to know the expectation value of the z-component of the nuclear angular momentum, $\langle J_z \rangle$, because transitions that change $\langle J_z \rangle$ a large amount are strongly suppressed. Figure 1 is a plot of the ground state doublet and the first excited state eigenvalues plotted against the expectation values $\langle J_z \rangle$. The value of $\langle J_z \rangle$ is written next to each point. The values for $\langle J_z \rangle$ are uniformly half integer as we would expect. Note that the scale of the $\langle J_z \rangle$ axis on the top of the plot is one tenth that of the bottom to show the form of the excited state more clearly. Figure 2 is similar to Figure 1 but with a magnetic field turned on in the z direction. The field used here is about 0.3 T, equal to that which would be generated internally by LiHoF_4 at zero temperature. As we will discuss, only transitions between energy levels with $I = 0$ will be included in our computations.

There is one important note here about the energy eigenvalues in our particular case. The crystal field parameters measured by Giffelman et al.⁸ were measured through high resolution optical spectroscopy and they did not observe the 9.5 K excited state in their luminescence spectra. Their parameters inserted into the calculation therefore predict that this unconstrained level sits at 14.5 K above the ground state doublet. Since this is the only state selected, we adjust our eigenvalues by subtracting 5 K from this state before using them in further calculations.

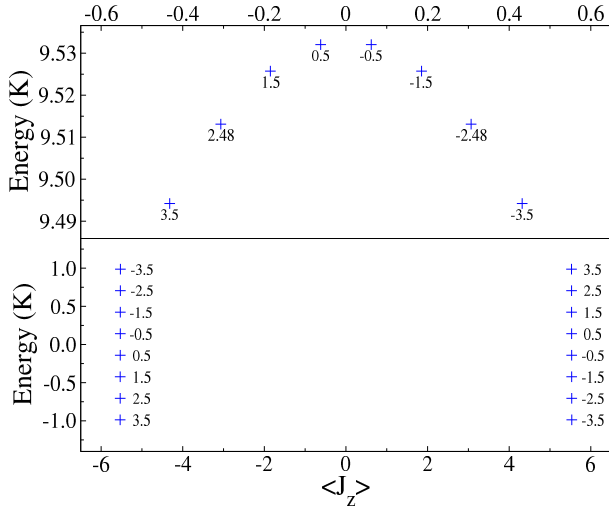


FIG. 1: Plot of the energy eigenvalues arranged in terms of the $\langle J_z \rangle$ expectation values. The labels on the points are the $\langle J_z \rangle$ expectation values. The bottom plot shows the ground state doublet, and the top plot is the 1st excited state.

Recall that the goal is to calculate a temperature dependent mean free path, $l(!)$, that is to be inserted in to the integral in equation 4. In the present case, we

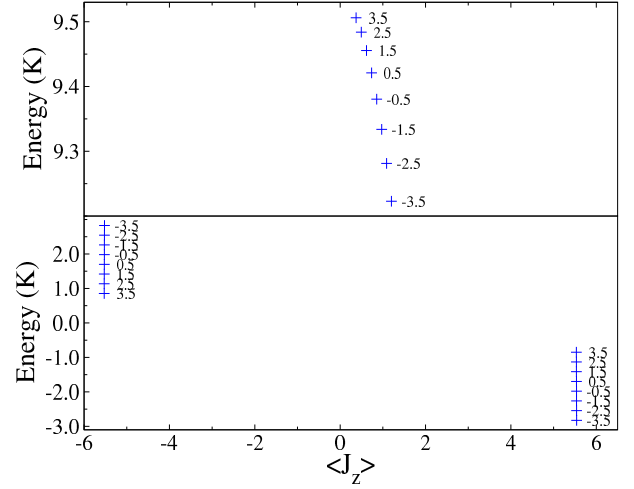


FIG. 2: Similar to Figure 1 but with magnetic splitting equal to what would occur in LiHoF_4 at 0 K. Note that the scale of the $\langle J_z \rangle$ axis is the same in the top and bottom of the plot.

assume that there are only three scattering processes, giving us three independent l 's to add. The first is due to phonon scattering from the sample boundaries. This term is simply the geometrically averaged sample size, l_{br} , and is independent of $!$. The second term is from scattering off of point defects, l_{pd} , which gives a term proportional to $l = !^4$ (see table II). As we shall see, this term is necessary to obtain agreement with the high temperature range of our data (though higher dimensional defects might also suffice, we assume point defects for simplicity). The last process is due to the non-trivial scattering from the Ho^{3+} ions, l_{ion} . Therefore,

$$l = \frac{1}{\frac{1}{l_{br}} + \frac{1}{l_{pd}} + \frac{1}{l_{ion}}} : \quad (10)$$

We choose to write the mean free path due to the single ion scattering process as $l_{ion} = l_{min} P_{scatt}$. The scale factor l_{min} is similar to the minimum distance that a phonon can go without running into a Ho^{3+} ion, and P_{scatt} is the probability that the phonon will scatter off of that ion. We define $l_{pd} = \frac{!^4}{1}$, and will use $!$ as a fitting parameter. Our complete expression for the mean free path is then

$$l(!) = \frac{1}{\frac{1}{l_{br}} + \frac{!^4}{1} + \frac{P_{scatt}(!;T)}{l_{min}}} : \quad (11)$$

After computing the energy level spectrum at a particular temperature, we calculate the partition function which is obtained by simply summing over each level, E_i , integrated over the level density, $D_i(!)$,

$$Z = \sum_i \int_0^Z \frac{1}{!} e^{-\frac{E_i}{!T}} D_i(!) d! : \quad (12)$$

We assume that the individual energy levels are thermally broadened (due to crystal field fluctuations from thermal motion of the atomic neighbors of the Ho^{3+} ions in the lattice) with a Gaussian energy distribution. For simplicity, we further assume that all of the levels are have the same width, E , resulting in the following energy density function,

$$D_i(\epsilon) = \frac{1}{E} e^{-\frac{(\epsilon - E_i)^2}{E^2}}; \quad (13)$$

Our partition function now becomes

$$Z = e^{\frac{2}{4} E^2 X} \sum_i e^{-E_i}; \quad (14)$$

The scattering probability, $P_{\text{scatt}}(E_P; T)$, is a function of the phonon energy, $E_P = \hbar\omega$, and the temperature of the system, T . We calculate it by performing a double sum over all the energy levels, calculating the scattering probabilities between each pair.

$$P_{\text{scatt}}(E_P; T) = \frac{\sum_{i,j} \langle I_z^{(i)} | I_z^{(j)} | \rangle}{Z^2} \sum_i e^{-D_{ij}(\epsilon)} \sum_j e^{-D_{ji}(\epsilon)}; \quad (15)$$

where $D_{ij}(\epsilon) = D_i(\epsilon) D_j(\epsilon + E_P)$ and $D_{ji}(\epsilon) = D_j(\epsilon) D_i(\epsilon - E_P)$. This particular form takes into account stimulated emission from the higher level to the lower one as well as the direct excitation of the ion. The delta function allows for excitations only between levels that have the same nuclear angular momentum expectation values (see Figs 1 and 2). Slightly decreasing this selectivity, say by allowing $\langle I_z^{(i)} | I_z^{(j)} | \rangle$ to vary by one or two, makes little difference to the current model except at the lowest temperatures (< 100 mK). Using the level density mentioned above, the scattering probability is found to be

$$P_{\text{scatt}}(E_P; T) = \frac{1}{Z} \sum_{i,j} e^{-\frac{1}{2} E^2} \sum_{\epsilon} e^{-\frac{(\epsilon - E_i - E_j + E_P)^2}{2 E^2}} e^{-\frac{1}{2} E^2 (E_i + E_j)} \langle I_z^{(i)} | I_z^{(j)} | \rangle; \quad (16)$$

The energy level width, E , requires attention here. The thermal energy due to deformation of the lattice is essentially

$$E_T = k_B T = \frac{1}{2} C_0 \epsilon^2; \quad (17)$$

where C_0 is an averaged elastic constant, and ϵ is an averaged strain. For small lattice deformations changes in the crystal field energy are therefore proportional to the strain,

$$E_{CF} / \epsilon = \text{constant}; \quad (18)$$

We collect the constants, and designate the thermal broadening as

$$E = A \sqrt{\frac{P}{T}}; \quad (19)$$

with A as a fitting parameter.

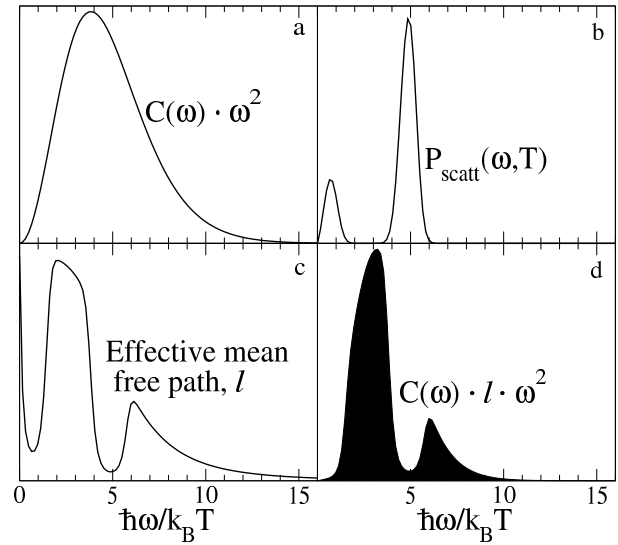


FIG. 3: Plots of the contributions to the heat capacity calculation for $T = 2$ K. The various panels are described in the text.

The thermal conductivity is calculated at each temperature by the following procedure. First the various temperature dependent parameters (internal field for LiHoF_4 and the broadening parameter A) are set and the Hamiltonian eigenvalue problem is solved. The integral in equation 4 is computed by inserting the mean free path, $l(\omega)$, from equation 11. The scattering probability is then calculated at each point in the integral using equation 16 where $E_P = \hbar\omega$.

We have used an integration cut-off of $\omega = 16 k_B T = \hbar$, which is quite sufficient as seen in Figure 3. Panel a is the heat capacity part of the integrand which essentially vanishes for higher frequencies. Panel b is the scattering probability from equation 16, and panel c is $l(\omega)$ from equation 11. The last panel, d, is the integrand to equation 4, so the area of the filled portion represents the total thermal conductivity at this temperature. The effect of transitions between Ho^{3+} levels is quite apparent in the mean free path data, effectively removing specific frequency bands from the thermal conductivity integral.

IV. EXPERIMENTAL DETAILS

Thermal conductivity was measured by the standard gradient method using a heater and two thermometers. Our heaters were 200 μ m metal film on Kapton strain gauges and the thermometers used were 1 k Ω to 10 k Ω RuO₂ surface mount resistors, depending on the temperature range of interest. Copper bars approximately 150 μ m thick were silver epoxied to the sample dividing it approximately into thirds. These bars defined the distance over which the temperature gradient, $T = T_2 - T_1$, was measured. The heaters were wired with superconducting NbTi wires to eliminate ohmic heating and to minimize heat leaks, while thin Evanohm wires were used on the thermometers. To check for thermal leakage through the wires, the measurement of LiY_{96%}Ho_{4%}F₄ was repeated with the wires doubled in length. The results of the thermal conductivity between the two sets of measurements were within the noise of either experiment. Our two samples (pure and dilute) were optically oriented and cut such that the long length was along the c axis. The pure LiHoF₄ was 1.46 \times 1.56 \times 5.4 mm³. This gives a cross section of 0.0228 cm². The distance, L , between the thermometers was 0.22 cm. The 11.7 mg dilute LiY_{96%}Ho_{4%}F₄ sample was 0.93 \times 0.75 \times 4.7 mm³, but slightly trapezoidal. The effective cross section was calculated by using measurements from a digital photograph of the sample. The final value used was $A = 0.0066$ cm². The distance between thermometers for this sample was also 0.22 cm. Most experiments were conducted in a ³He cryostat. Data below 310 mK were obtained in a helium dilution refrigerator.

V. EXPERIMENTAL RESULTS

A. Pure LiHoF₄

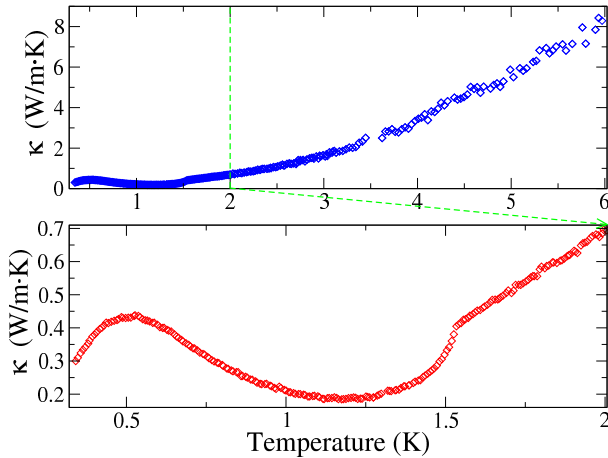


FIG. 4: Measured thermal conductivity, κ , for LiHoF₄. The bottom panel is a magnification of the top to better illustrate the structure below the Curie temperature, T_C .

The accumulated data for a number of experiments are plotted in figure 4. The top panel is the entire range of data obtained, and the bottom panel is a magnification of data below 2 K. One can easily see the ferromagnetic transition on this plot at 1.54 K. One interpretation of the overall structure of the data is as follows; as we go down in temperature, the thermal conductivity decreases due to the T^3 term in the specific heat. At this point, the vast majority of phonon-driven transitions are between the hyperfine ground state sublevels. When we reach T_C , the ground states start Zeeman splitting, and there are a number of new transition possibilities opened up, so the conductivity drops rapidly. Note that the peak in $C(\omega)$ in figure 3 occurs at approximately $\omega = 4k_B T = \hbar$. This implies that at T_C , about 1.5 K, the majority of phonons have energies around 6 K. However, just above T_C , the Ho³⁺ energy spectrum looks like that shown in figure 1, where there are no scattering possibilities for phonons between about 2 K and about 8.5 K. Below T_C , the excluded temperature region quickly shrinks due to the splitting, and simultaneously, the peak of the phonon spectrum decreases. At about 1.2 K, the ground states have split enough that transitions are suppressed and the conductivity starts increasing. Eventually, this rise is expected to be countered by the T^3 factor from having a sample of finite size. While this qualitative explanation was the primary motivation to develop a single ion model of the thermal conductivity we shall see that this picture is not sufficient to explain all of the data.

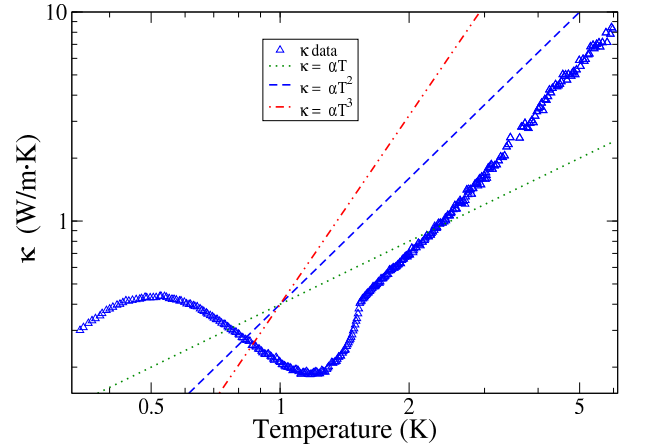


FIG. 5: log-log plot of κ for LiHoF₄ along with some lines of T^n for comparison with table II.

Figure 5 shows the whole range of data on a log-log plot, along with lines proportional to T , T^2 , and T^3 . Recall from table II the various structural scattering processes that can contribute to the thermal conductivity. As one can see, the data do not follow any one of these power laws over any significant temperature range. We did not take measurements of the pure LiHoF₄ in the dilution refrigerator, so we can not see the approach to T^3 in the low temperature limit.

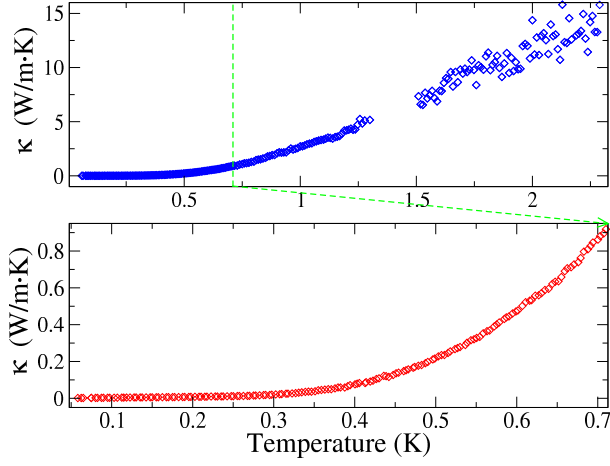


FIG. 6: Measured κ for $\text{LiY}_{96\%}\text{Ho}_{4\%}\text{F}_4$. The bottom panel is a magnified view of the top.

B. Dilute $\text{LiY}_{96\%}\text{Ho}_{4\%}\text{F}_4$

We have again plotted our data in two temperature ranges in figure 6. This plot is not very illuminating by itself since it goes so quickly and smoothly to zero. There is no ferromagnetic transition, so there are no sharp structures as there are for LiHoF_4 . (The gap in the data between 1.3 K and 1.5 K is due to T-control issues in the ^3He cryostat.) As in the previous section, the data becomes increasingly noisy at higher temperatures due to the reduced sensitivity of the thermometers and the rapidly increasing thermal conductivity. Note that at 2 K the thermal conductivity of $\text{LiY}_{96\%}\text{Ho}_{4\%}\text{F}_4$ is about 10 times that of LiHoF_4 , but slightly smaller at 0.5 K.

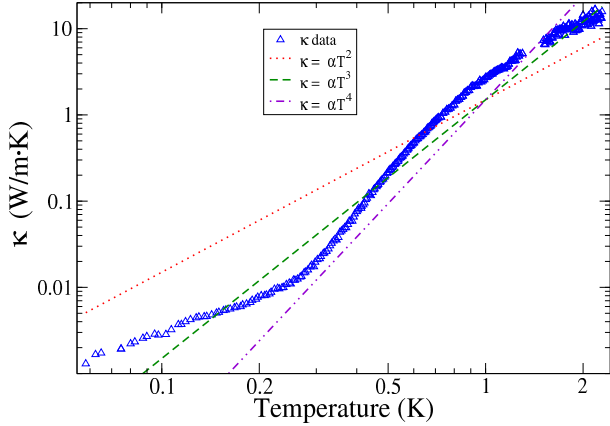


FIG. 7: log-log plot of κ for $\text{LiY}_{96\%}\text{Ho}_{4\%}\text{F}_4$ along with some T^n lines for comparison.

Figure 7 is a plot of $\log(\kappa)$ versus $\log(T)$ to check for regions where the thermal conductivity is dominated by a single power law. It appears that at the lowest temperatures the data may be approaching T^3 , but going to lower temperatures would be necessary to confirm this.

More importantly, the log plot brings out structures that must be reproduced by our single-ion model if it is to describe the data.

VI. ANALYSIS

Our goal is to find a set of parameters that provide the best fit for both our LiHoF_4 and $\text{LiY}_{96\%}\text{Ho}_{4\%}\text{F}_4$ data simultaneously. Fitting parameters include β , which determines the contribution from point defect scattering, and l_{min} , which determines the size of the contribution from the Ho^{3+} ion scattering. P_{scatt} also contains a parameter that can be varied, as does the thermal broadening, Eq. 19. Since A is a single ion property, it should be independent of the concentration of the Ho^{3+} ions. Similarly, l_{min} should be proportional to the inverse of the cube root of the concentration, fixing its relative value. The effective mean free path due to the finite size of the sample, l_{br} , is calculated from the sample dimensions and is fixed. We take A_J from equation 9 to be a constant, 38.6 mK, since this value has been measured and published using at least two different methods^{10,11}. As mentioned, $H_0 = 0.33\text{T}$ from equation 8 was indirectly, and somewhat imprecisely, measured by Battison et al.⁴.

We will first discuss the dilute glassy system $\text{LiY}_{96\%}\text{Ho}_{4\%}\text{F}_4$.

A. Dilute $\text{LiY}_{96\%}\text{Ho}_{4\%}\text{F}_4$

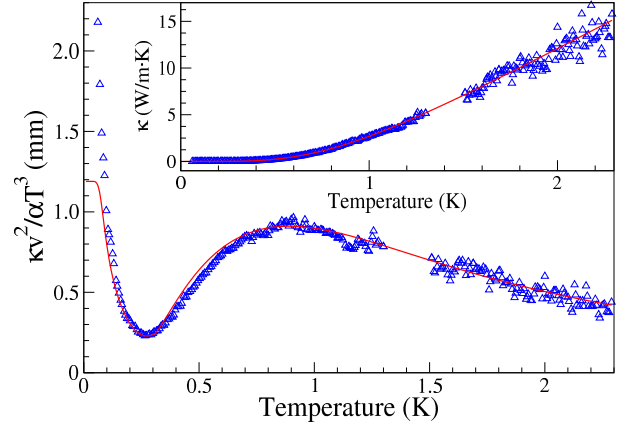


FIG. 8: Plot of $\kappa v^2 = T^3$ and best fit for $\text{LiY}_{96\%}\text{Ho}_{4\%}\text{F}_4$. Inset is κ .

Figure 8 is a plot of $\kappa v^2 = T^3$ for $\text{LiY}_{96\%}\text{Ho}_{4\%}\text{F}_4$ along with the best model fit. Here,

$$\kappa v^2 = \frac{2}{15} \frac{k_b^4}{h^3} \quad (20)$$

which gives us $\kappa v^2 = T^3$ roughly in units of the mean free path (the equivalence would be exact if l did not depend on T). As we can see, the fit is quite good with

this parameter set. The best fit parameters are $A = 0.45 \text{ } 0.03 \text{ K}^{-1/2}$, $l_{\text{min}} = 38 \text{ } 1 \text{ m}$, and $\xi = 15 \text{ } 2 \text{ m K}$. The uncertainties were estimated by varying the individual parameters to obtain the same minimum χ^2 , and do not reflect any correlations between the parameters. As we can see, the scattering due to point defects is a fairly small contribution. For example, a 1 K phonon will have a mean free path, due to this process, of about 15 m eters. Only for phonons with energies greater than about 12 K does the mean free path become smaller than the physical size of the sample. Because of this, the initial fitting was done with $\xi = 1$, after which ξ was adjusted to minimize the χ^2 .

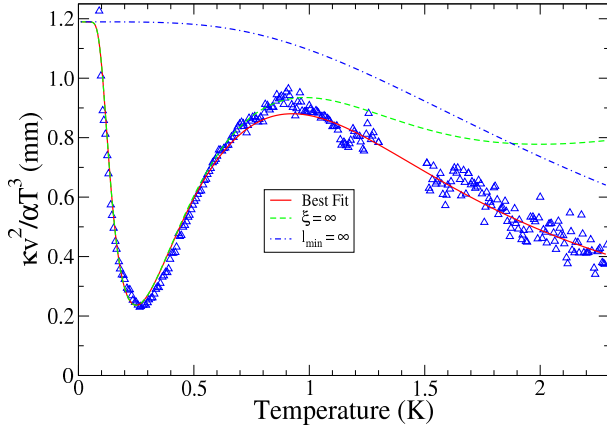


FIG. 9: Plot of $v^2 = T^3$ and variations on the best fit for $\text{LiY}_{96\%}\text{Ho}_{4\%}\text{F}_4$. The parameters are described in the text.

Figure 9 demonstrates how each parameter effects the model. Unless noted, all lines shown here use the "best fit" parameters. The dashed line has the point defect scattering turned on by setting $\xi = 1$. Note that this line follows the best fit line fairly well for temperatures below the peak at 900 mK , and is identical for temperatures less than 500 mK . The dot-dashed line demonstrates the effect of turning on the Ho^{3+} single ion scattering process by setting $l_{\text{min}} = 1$. If we turned on the point defect scattering at the same time, we would obtain a horizontal line at $v^2 = T^3 = l_{\text{br}} = 1.19 \text{ m}$. From this, we see that the single ion process alone is responsible for the structure of the dip at 270 mK and the addition of the point defect scattering causes a turn-over in the data to produce the peak at 900 mK .

In the very low temperature region, less than 80 mK , the model demonstrates a flattening behavior that is not present in the data. This is due to the value of l_{br} , since it sets the overall maximum mean free path. Interestingly, increasing l_{br} beyond its physical value does not improve the overall model, as this effectively scales the entire fit. There currently is no parameter set in with this model that reproduces the $T < 80 \text{ mK}$ region while retaining agreement with the rest of the data set. One explanation for this could be related to the surface condition of the sample. At very low temperatures, phonons

will have an increasing wavelength, which will eventually become larger than the surface roughness. When this occurs, the boundary scattering becomes specular and the effective mean free path due to the finite size of the sample increases. This would result in a rapid upturn of $v^2 = T^3$ when this limit is reached, consistent with our measurements.

We believe that this single ion model describes the thermal conductivity of $\text{LiY}_{96\%}\text{Ho}_{4\%}\text{F}_4$ fairly well below 2.5 K , and demonstrates the relative importance of scattering from point defects. We see no sign of the "cluster glass" proposed by Reich et. al². They observed narrowing in the magnetic susceptibility with decreasing temperatures between 300 mK and 150 mK , but we see no signs of collective behavior in this temperature range.

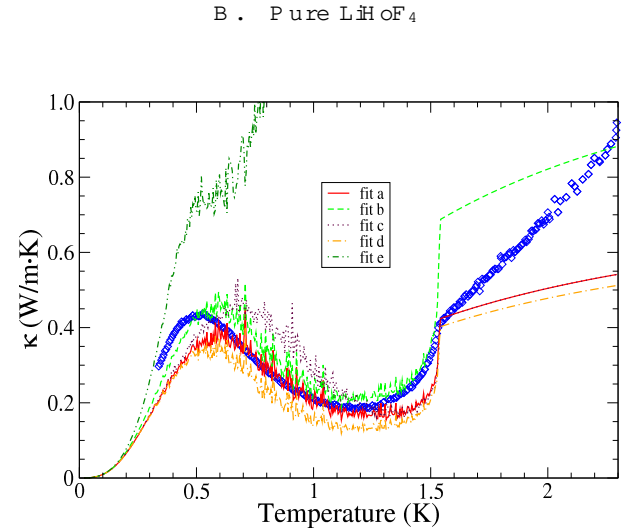


FIG. 10: Plot of $v^2 = T^3$ and three fits for LiHoF_4 . Parameters are described in the text.

We now move to the ferromagnet LiHoF_4 . Because A should be independent of the concentration of the Ho^{3+} ions, and l_{min} should be proportional to the inverse of the cube root of the concentration, we will start with $A = 0.45 \text{ K}^{-1/2}$, $l_{\text{min}} = \sqrt[3]{4\%} \cdot 38 = 13 \text{ m}$, and $\xi = 15 \text{ m K}$. from the analysis of $\text{LiY}_{96\%}\text{Ho}_{4\%}\text{F}_4$. We also turn on the Zeeman splitting by setting H_0 from equation 8 to 0.33 T . Figure 10 is a plot of $v^2 = T^3$ versus temperature for LiHoF_4 with three lines from our model. Note that the vertical axis is on a log scale so that the structure of the ferromagnetic transition can be seen. The solid line is our "best fit" with the above parameters. The dashed line uses the same parameters except for $\xi = 1$ to see the effect of turning on the point defect scattering. The dot-dashed line has $l_{\text{min}} = 1$ to demonstrate the effect of turning on the Ho^{3+} single ion scattering contribution (the individual contributions are more profitably viewed using the color figure available online). As we can clearly see, the "best fit" is poor. Furthermore, no amount of adjustment of the

parameters appears to yield significantly better agreement. We do, however, see some qualitative successes with this model of LiHoF_4 . The behavior immediately below the Curie temperature is generally what we predicted from section V A and we see a reasonably accurate roll-off in $\chi = T^{-3}$ at the lowest temperatures. One possibility is that there are one or more additional scattering mechanisms needed in the model. For example, below the Curie temperature, domain formation could introduce a temperature dependent grain boundary-like scattering process. However, this would have no effect above T_C , where the deviation from the fit is most pronounced. (Of course, it is possible that difficulties present below T_C in the model result in best-fit deviations above the Curie point.) The second, and potentially most interesting possibility is that phonon-excited spatially correlated spin- $\frac{1}{2}$ pairs account for the enhanced scattering. Note that, unlike isotropic or nearly isotropic systems, conventional

spin-waves are not expected in an ensemble of Ising spins. Indeed, the nature of (potentially collective) magnetic excitations above and below T_C in this dipolar-coupled system are unclear, as is the question of whether such magnetic scattering could account for the behavior we observe. Again, one would naively believe such effects to strongly dominate below T_C . At higher temperature it is unclear what multi-spin excitations are available to couple to the phonon current.

In conclusion, a detailed semi-phenomenological model of single-ion phonon scattering processes is in excellent agreement with thermal conductivity data on dilute $\text{LiY}_{96\%}\text{Ho}_{4\%}\text{F}_4$, with no evident signature of low-energy collective excitations involving random spin clusters. Similar data on the pure ferromagnetic system LiHoF_4 , however, are not in quantitative agreement with the independent ion theory and will presumably require a study of collective effects in this dipolar Ising system.

Present address: Yale University, Sloane Physics Lab, New Haven, CT

^y Electronic address: belman@kent.edu

¹ D. H. Reich and T. F. Rosenbaum, *Physical Review Letters* 59, 1969 (1987).

² D. H. Reich, B. Ellman, J. Yang, T. F. Rosenbaum, G. Aeppli, and D. P. Belanger, *Physical Review B* 42, 4631 (1990).

³ P. G. Klemens, *Solid State Physics* (Academic Press Inc., 1958), vol. 7, chap. Thermal Conductivity and Lattice Vibrational Modes, pp. 1{99.

⁴ J. E. Battison, A. Kasten, M. J. M. Leask, J. B. Lowry, and B. M. Wanklyn, *Journal of Physics C: Solid State Physics* 8, 4089 (1975).

⁵ R. G. Iraud, W. W. emsdorfer, A. M. Tkachuk, D. M. ailly, and B. Barbara, *Physical Review Letters* 87, 057203 (2001).

⁶ K. W. H. Stevens, *Proceeding of the Physical Society* 65A, 209 (1952).

⁷ M. T. Hutchings, *Solid State Physics* (Academic Press Inc., 1964), vol. 16, chap. Point-Charge Calculations of Energy Levels of Magnetic Ions in Crystalline Electric Fields, pp. 227{273.

⁸ S. N. G. ifeism an, A. M. Tkachuk, and V. V. Prizmak, *Optical Spectroscopy* 44, 68 (1978).

⁹ J. A. Gri n, M. Huster, and R. J. Folweiler, *Physical Review B* 22, 4370 (1980).

¹⁰ G. Mennenga, L. de Jongh, and W. H. uiskamp, *Journal of Magnetism and Magnetic Materials* 44, 59 (1984).

¹¹ J. M. agarino, J. Tuchendler, J. P. D'Haenens, and A. Linz, *Physical Review B* 13, 2805 (1976).